

# Cut-Off Circular Waveguide Method for Dielectric Substrate Measurements in Millimeter Wave Range

Takashi SHIMIZU<sup>†a)</sup>, Student Member and Yoshio KOBAYASHI<sup>†</sup>, Fellow

**SUMMARY** A novel resonator structure for the cut-off circular waveguide method is proposed to suppress the unwanted TE modes in the axial direction and TM modes in the radial direction. In this method, a dielectric plate sample is placed between two copper circular cylinders and clamped by two clips. The cylinder regions constitute the  $TE_{0m}$  mode cut-off waveguides. The measurement principle is based on a rigorous analysis by the Ritz-Galerkin method. Many resonance modes observed in the measurement can be identified effectively by mode charts. In order to verify the validity of the novel structure for this method, the temperature dependences for three low-loss organic material plates were measured in the frequency range 40 to 50 GHz. It is found that modified polyolefin plates have comparable electric characteristics and low price, compared with PTFE plates. Moreover, it is verified that the novel resonator structure is effective in improvement of accuracy and stability in measurement. The measurement precisions are estimated within 1 percent for  $\epsilon_r$  and within 15 percent for  $\tan \delta$ .

**key words:** cut-off circular waveguide method, millimeter wave, dielectric substrate measurement

## 1. Introduction

Recently, the development of new material with low-loss characteristics and low price is requested for application to millimeter wave circuit. It has been an important subject to measure complex permittivity of dielectric materials accurately and efficiently in millimeter wave range. Some measurement methods [1]–[3] have been reported to evaluate these dielectric materials in millimeter wave range.

In our laboratory, we have proposed a cut-off circular waveguide method to measure the temperature dependence of complex permittivity of low-loss dielectric plates accurately and efficiently in the millimeter wave range [4]–[10].

At first, a  $TE_{011}$  mode circular waveguide method was proposed by S.B. Cohn and K.C. Kelly [11], where a resonator is constituted by inserting a circular disk sample into a  $TE_{01}$  mode cut-off circular waveguide. This method was applied with a waveguide excitation to the millimeter wave measurement [12]. In order to measure any size of samples nondestructively, a novel resonator structure, where a dielectric plate sample is placed between two copper circular cylinders, was proposed by Y. Kobayashi and J. Sato [4], and G. Kent [13], independently. However, it was found that the correction value of the fringe effect for relative permittivity by the G. Kent's method was not correct.

The features of the cut-off circular waveguide method

are as follows,

- The measurement principle is based on rigorous analysis by the Ritz-Galerkin method with the mode matching technique [4], [5].
- The dielectric plate sample is placed between two cylinders into which a copper circular cylinder is cut in the middle of height and clamped by two clips; hence, the sample can be exchanged easily [6].
- The millimeter wave vector network analyzer constituted by a coaxial cable system is used; hence, it is easy to adjust the coupling strength finely.
- A mode chart is presented to identify many resonance modes observed in the measurement [7].
- An automatic measurement system was developed to measure the temperature dependence more efficiently and precisely [8].
- A grooved circular cavity for separating degenerate TE and TM modes to measure the dimension and relative conductivity accurately is presented [9].

Recently, we found that the unwanted TE modes in the axial direction and TM modes in the radial direction are excited in the conventional structure [14]. These resonance modes affect the complex permittivity measurements.

In this paper, a novel resonator structure for the cut-off circular waveguide method is proposed to suppress the unwanted TE modes in the axial direction and TM modes in the radial direction, respectively. The validity of correction for the fringe effect by the rigorous analysis is confirmed experimentally. In order to verify the validity of the novel resonator structure for this method, the temperature dependences of complex permittivity for three low-loss organic material plates are measured for the  $TE_{011}$  mode in the frequency range 40 to 50 GHz.

## 2. Measurement Principle

### 2.1 Resonator Structure

A novel resonator structure is shown in Fig. 1(a). A copper circular cylinder with the diameter  $D$  is cut into two parts in the middle of the height  $H$ . A dielectric plate sample having the thickness  $t$  and the diameter  $d$ , which is larger than  $D$ , is placed between these cylinders and clamped by two clips. The cylinder regions constitute the  $TE_{0m}$  mode cut-off waveguides; hence, the fields decay exponentially in the axial direction. Similarly, the dielectric plate region outside  $D$

Manuscript received September 2, 2003.

Manuscript revised December 4, 2003.

<sup>†</sup>The authors are with the Faculty of Engineering, Saitama University, Saitama-shi, 338-8570 Japan.

a) E-mail: shimizu@reso.ees.saitama-u.ac.jp

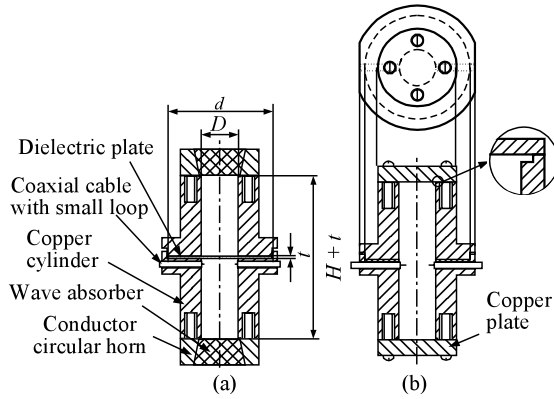


**Fig. 1** Cross sectional view of resonator structures used for measurements. (a) Circular cylindrical resonator clamping a dielectric plate. (b) Circular empty cavity.

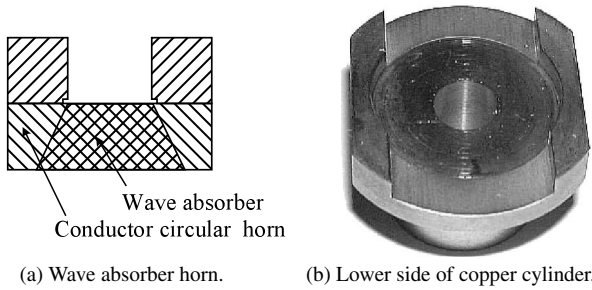


**Fig. 2** Structure of two novel parts in the resonator.

constitutes a radial cut-off waveguide; hence, the fields decay rapidly in the radial direction. There are two novel parts in this resonator.

Conductor circular horns with wave absorbers as shown in Fig. 2(a) are attached at both ends of the circular cylinder. These parts suppress the unwanted TE modes propagated forth and back in the axial direction.

The lower side of copper cylinder opened a half part by machining on which a sample is placed is shown in Fig. 2(b). This structure suppresses the unwanted TM modes propagated forth and back in the radial direction.

This resonator is excited and detected at the middle of the cylinder by a pair of UT-47 semi-rigid coaxial cables (outer diameter 1.2 mm) with small loops at the top.

## 2.2 Relative Permittivity $\epsilon_r$ Measurement

The axially symmetric  $TE_{0m1}$  ( $m = 1, 2, \dots$ ) modes are used to avoid air gap effects at the plate-cylinder interface [7]. The values of relative permittivity  $\epsilon_r$ , in consideration of the fringe effect, can be calculated accurately from the measured values of resonance frequency,  $f_0$  and unloaded  $Q$ ,  $Q_u$  of the  $TE_{0m1}$  mode. The formula is given by,

$$\det H(f_0; \epsilon_r, D, t, d, \epsilon_g, g) = 0 \quad (1)$$

where  $g$  is a gap between the sample and the cylinder and  $\epsilon_g$  is relative permittivity of the gap. The derivation of this formula is given in Appendix A.1, since original derivation

presented in [4] is not well known.

## 2.3 Loss Tangent $\tan \delta$ Measurement

The values of loss tangent  $\tan \delta$ , in consideration of the fringe effect, can be calculated accurately from the measured values of  $Q_u$  of the  $TE_{0m1}$  mode. The formula is given by,

$$\tan \delta = A/Q_u - BR_s \quad (2)$$

where  $R_s = \sqrt{\pi f_0 \mu_0 / \sigma}$  is surface resistance of the cylinder,  $\sigma = \sigma_0 \sigma_r$  is the conductivity,  $\sigma_0 = 58 \times 10^6$  S/m is the conductivity of the standard copper,  $\sigma_r$  is the effective relative conductivity, including influence of oxidation and roughness of the copper surface and  $\mu_0 = 4\pi \times 10^{-7}$  H/m is the permeability in the vacuum. Also  $A$  and  $B$  are constants calculated from the frequency changes due to each perturbation of  $\epsilon_r$ ,  $D$  and  $g$  for  $\epsilon_g = 1$  by using Eq. (1), that is,

$$A = -\frac{f_0}{2\epsilon_r} \frac{\Delta \epsilon_r}{\Delta f_{0\epsilon}} \quad (3)$$

$$B = \frac{1}{120\pi k_0 \epsilon_r} \frac{\Delta \epsilon_r}{\Delta f_{0\epsilon}} \left( \frac{\Delta f_{0D}}{\Delta D} + \frac{\Delta f_{0g}}{\Delta g} \right) \quad (4)$$

The derivations of these formulas are given in Appendix A.2, since original derivations presented in [5] are not well known.

## 2.4 Measurement Error

The mean square error of  $\epsilon_r$ ,  $\Delta \epsilon_r$  is mainly determined by the errors of measured  $D$ ,  $t$  and  $f_0$  values, that is,

$$\Delta \epsilon_r^2 = \Delta \epsilon_D^2 + \Delta \epsilon_t^2 + \Delta \epsilon_f^2 \quad (5)$$

with

$$\Delta \epsilon_D = \frac{\partial \epsilon_r}{\partial D} \Delta D, \quad \Delta \epsilon_t = \frac{\partial \epsilon_r}{\partial t} \Delta t, \quad \Delta \epsilon_f = \frac{\partial \epsilon_r}{\partial f_0} \Delta f_0 \quad (6)$$

where  $\Delta D$ ,  $\Delta t$  and  $\Delta f_0$  are the mean square error of  $D$ ,  $t$  and  $f_0$ .

Likewise, the mean square error of  $\tan \delta$ ,  $\Delta \tan \delta$  is mainly determined by the errors of measured  $Q_u$  and  $\sigma_r$  values, that is,

$$\Delta \tan \delta^2 = \Delta \tan \delta_{Q_u}^2 + \Delta \tan \delta_{\sigma_r}^2 \quad (7)$$

with

$$\Delta \tan \delta_{Q_u} = \frac{\partial \tan \delta}{\partial Q_u} \Delta Q_u, \quad \Delta \tan \delta_{\sigma_r} = \frac{\partial \tan \delta}{\partial \sigma_r} \Delta \sigma_r \quad (8)$$

where  $\Delta Q_u$  and  $\Delta \sigma_r$  are the mean square error of  $Q_u$  and  $\sigma_r$ .

## 2.5 Determination of Dimension and Relative Conductivity

The values of  $D$ ,  $H$  and  $\sigma_r$  of a copper cavity can be determined by using a circular empty cavity shown in Fig. 2(b),

because the accurate value of  $D$  cannot be measured mechanically. In this case, copper plates are attached at both ends in place of the conductor circular horns with wave absorbers. The degenerate  $TM_{11p}$  mode can be separated from the  $TE_{01p}$  mode by grooves machined at both ends of the cylinders [9]. The values of  $D$  and  $H$  are determined from a couple of resonance frequencies  $f_{0p}$  and  $f_{0q}$  measured for the  $TE_{01p}$  and  $TE_{01q}$  ( $p \neq q$ ,  $p < q$ , integer) modes by using following equations [5],

$$D = \frac{c j'_{01}}{\pi} \sqrt{\frac{q^2 - p^2}{(q f_{0p})^2 - (p f_{0q})^2}} \quad (9)$$

$$H = \frac{c}{2} \sqrt{\frac{q^2 - p^2}{f_{0q}^2 - f_{0p}^2}} \quad (10)$$

where  $c$  is velocity of light and  $j'_{01} = 3.83171$ .

The value of  $\sigma_r$  is determined from the  $f_{0p}$  and  $Q_{up}$  values measured for the  $TE_{01p}$  mode by using following equation [5],

$$\sigma_r = \frac{4\pi f_{0p} Q_{up}^2 \left\{ j_{01}'^2 + 2(p\pi)^2 \left(\frac{D}{2H}\right)^3 \right\}^2}{\sigma_0 \mu_0 c^2 \left\{ j_{01}'^2 + \left(\frac{p\pi D}{2H}\right)^2 \right\}^3} \quad (11)$$

### 3. Discussions of the Fringe Effect

#### 3.1 Convergence on the Solution

As the number of the matrix  $N$  and the variable  $K$  for Eq. (1) are increased, the solution approaches true values. In actual calculations,  $N$  and  $K$  are chosen so that the solution has an accuracy of five significant figures because of the reduction of calculation time. Figure 3 shows the calculation results of  $f_0$  for  $\epsilon_r = 2$  and  $t = 0.5$  mm with the  $TE_{0m1}$  ( $m = 1, 2, 3$ ) modes. As the order of  $m$  is increased, the convergence is slower. Those behaviors of the convergence shows similar tendency. In case of  $N = 20$  and  $K = 40$  for  $TE_{011}$  mode, we obtain the accuracy of five significant figures for the solution of  $f_0$ . Moreover, calculation time is about 1 second using

Pentium II<sup>®</sup> 500 MHz. If  $N = 80$  and  $K = 80$  are used, it is about 50 seconds. In our methods,  $N = 20 + 4 \cdot (m - 1)$  which is empirical formula and  $K = 40$  is determined.

#### 3.2 The Experiment of the Fringe Effect

We performed experiments to verify the calculations for the fringe effect. The complex permittivity of PTFE plates with  $t = 1.997, 2.499$  and  $3.007$  mm is measured around 20 GHz for  $TE_{011}$  mode by using the cylinder with  $D = 16.597$  mm,  $H = 83.268$  mm and  $\sigma_r = 86.0\%$ . Figure 4 shows the measured results of three PTFE plates, where  $\epsilon_a$  and  $\tan \delta_a$  are the value neglecting the fringe effect,  $\epsilon_r$  and  $\tan \delta$  are considering one by this paper and  $\epsilon_k$  is considering one by G. Kent's method [13]. According to the reference [13], the correction value of the fringe effect is presented as follow:

$$\frac{\Delta \epsilon_k}{\epsilon_r} = \frac{4}{\pi \epsilon_r} \left( \frac{j'_{0m} c}{\pi f_0 D} \right)^2 \left\{ 1 - \epsilon_r \left( \frac{2 f_0 t}{c} \right)^2 \right\}^{-1/2} \left( \frac{t}{D} \right) \quad (12)$$

As the results,  $\epsilon_a$  and  $\tan \delta_a$  are increased as the  $t$  becomes thicker. However,  $\epsilon_r$  and  $\tan \delta$  are approximately con-

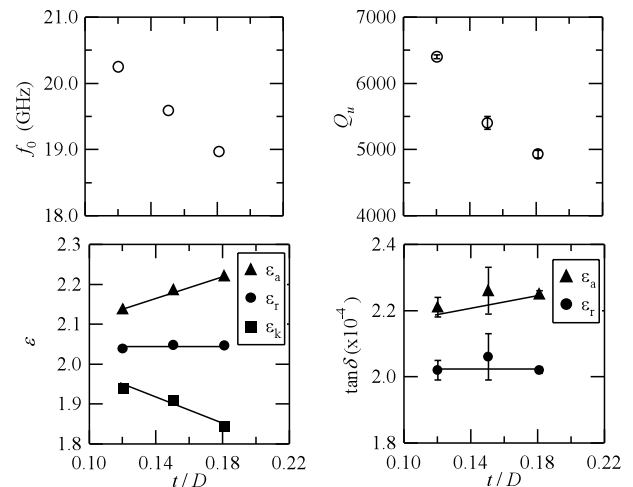


Fig. 4 Measured result of three PTFE plates by using the cylinder with  $D = 16.597 \pm 0.001$  mm,  $H = 83.268 \pm 0.004$  mm and  $\sigma_r = 86.0 \pm 3.0\%$ .

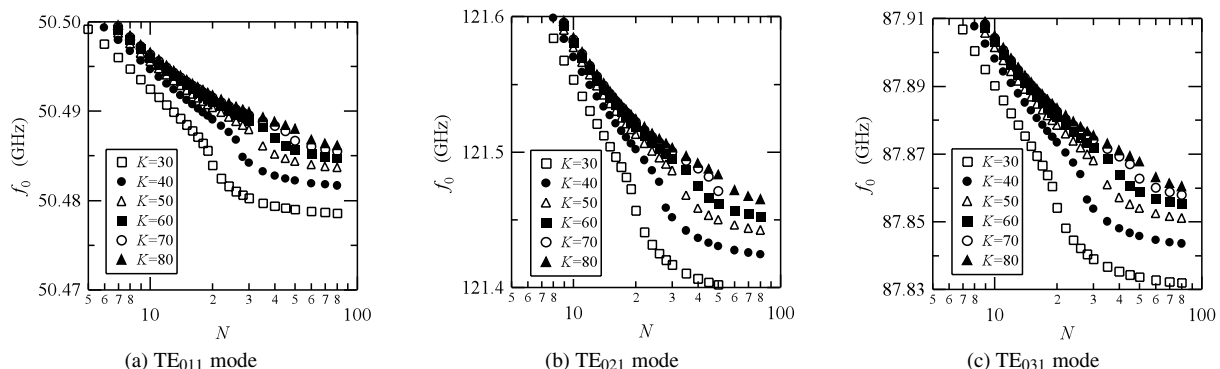


Fig. 3 The convergence of the solution for  $\epsilon_r = 2$  and  $t = 0.5$  mm with the  $TE_{011}$ ,  $TE_{021}$  and  $TE_{031}$  modes.

stant within the error. On the other hand,  $\epsilon_k$  is decreased, because the correction value is too much. In other word, Eq. (13) is not proper and the relational expression is expressed as follows,

$$\frac{\Delta\epsilon_r}{\epsilon_r} \cong \frac{1}{2} \frac{\Delta\epsilon_k}{\epsilon_r} \tag{13}$$

#### 4. Discussion for the Resonator Structure

We discuss the resonator structure to suppress unwanted resonance modes. The unwanted resonance modes are excited in the axial and radial directions, respectively. The resonant frequencies of these modes are determined from relative permittivity and thickness of a dielectric plate.

##### 4.1 Axial Direction

Two sapphire plates named as sample-A with  $t=0.298$  mm and sample-B with  $t=0.506$  mm are measured by using three resonators with the conventional absorbers [6]. The resonator I has  $D=6.991$  mm,  $H=30.917$  mm and  $\sigma_r=84.8\%$ , the resonator II has  $D=6.985$  mm,  $H=26.117$  mm and  $\sigma_r=76.2\%$  and the resonator III has  $D=6.480$  mm,  $H=24.289$  mm and  $\sigma_r=75.0\%$ .

The measured results are shown in Fig. 5. It is found that the  $\tan \delta$  value of the sapphire-A measured using the resonator I is considerably higher than other.

In the two cases of conventional wave absorbers and copper plates attached both ends of the cylinder, the frequency responses for the resonator I with the sapphire-A plate are shown in Fig. 6 by the long dash line and the

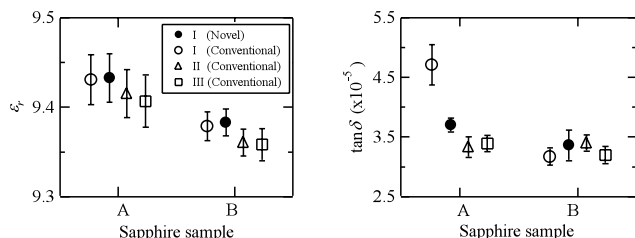


Fig. 5 Measured results for two sapphire plates (sample-A:  $t=0.298$  mm and sample-B:  $t=0.506$  mm).

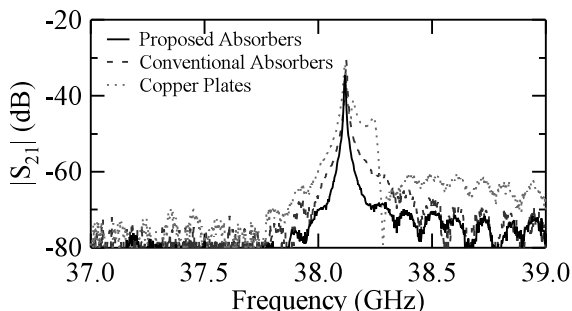


Fig. 6 The frequency responses for the resonator I with the sapphire-A plate attaching two type wave absorbers or copper plates.

dash line, respectively. When the conventional wave absorbers are attached, other resonance modes are not observed. When the wave absorbers are exchanged to the copper plates, it is found that the unwanted cavity mode exists around 38.2 GHz. We call this mode the TE mode in the axial direction [14]. As a result, the measured  $Q_u$  value decreases due to the influence of the unwanted TE mode because these conventional wave absorbers do not have sufficient attenuation to suppress them completely.

The novel structure of the wave absorber parts in the resonator to suppress the unwanted TE modes is shown in Fig. 2(a). The sapphire plates are measured by using the resonator I with the novel wave absorber horns. The measured results are shown in Fig. 5 by the circular mark. The frequency response is shown in Fig. 6 by the solid line. It is found that the value of  $\tan \delta$  of sapphire-A measured by using the resonator I with the novel wave absorber horns agree with the other results within measurement error 15 percent. The novel wave absorber horns are useful to suppress the unwanted TE modes.

##### 4.2 Radial Direction

The frequency responses of a modified polyolefin plate with  $t=1.165$  mm by using the conventional [6] and novel type resonators are shown in Fig. 7 by dash line and solid line, respectively. The resonance frequencies calculated from the mode chart for a simple resonator neglecting the fringe effect [6] are indicated on the top of Fig. 7. It is found the small resonance peaks at 12, 16, 30, 38, 41 and 48 GHz, which are not calculated from the mode chart, are excited by using the conventional resonator. We call these modes the TM modes in the radial direction [14]. These modes affect to measured value of the unloaded  $Q$  when these modes is close to the  $TE_{011}$  mode. On the other hand, the small resonance peaks are suppressed by using the novel resonator and the measured resonance frequencies agree with the one calculated from the mode chart. The novel resonator is useful to suppress the unwanted TM modes.

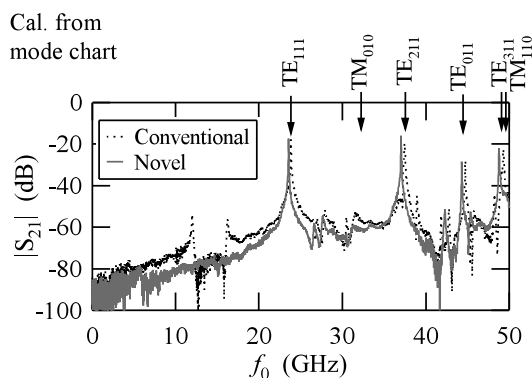
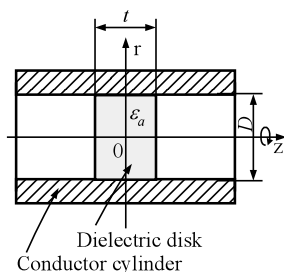


Fig. 7 The frequency responses of the modified polyolefin plate.

### 5. Identification of Resonance Modes

A program to make a mode chart for  $f_0$  versus  $\epsilon_a$  was developed on the basis of the characteristic equations [6] for a simple cut-off circular waveguide resonator without the fringe effect, as shown in Fig. 8, where  $f_0$  is the measured resonance frequency and  $\epsilon_a$  is an approximate relative permittivity when the fringe effect is neglected. The mode chart for  $D=6.991$  mm and  $t=2.050$  mm for a modified polyolefin



**Fig. 8** The cross sectional view of a simple circular cut-off waveguide resonator where the fringe effect is neglected.

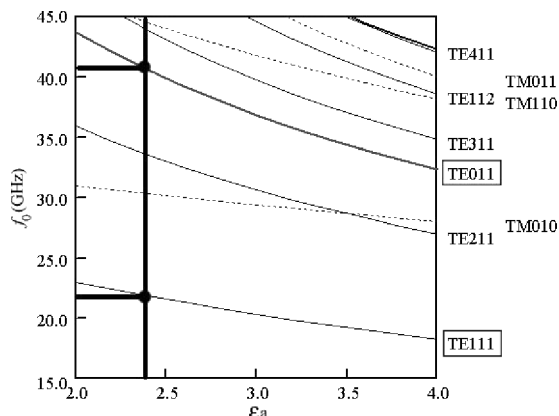


**Fig. 9** Mode chart of a dielectric disk resonator loaded in a circular cut-off waveguide calculated for  $D=6.991$  mm and  $t=2.050$  mm for a modified polyolefin plate.

Cal. from  
 $\epsilon_a=2.3$  and  
 $t=2.050$ mm

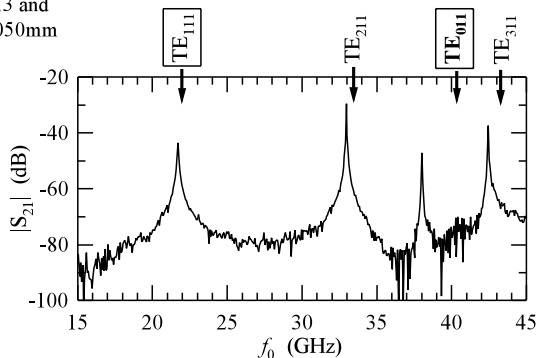


**Fig. 10** Frequency response measured for the modified polyolefin plate and resonance frequency calculated from the mode chart.

plate is shown in Fig. 9. This is more powerful to identify measured resonance modes, as described below. The frequency response for the modified polyolefin plate is shown in Fig. 10. Mode identification of these measured resonance peaks can be performed from the resonance frequencies calculated from the mode chart, indicated on the top of Fig. 10. In this case, it is found quickly from Fig. 9 that  $\epsilon_a$  is 2.3 from  $f_0$  of the dominant TE<sub>111</sub> mode and resonance frequencies of the TE<sub>011</sub> mode appear around 40 GHz.

### 6. Measurements

#### 6.1 Automatic Measurement System for Temperature Dependence

An automatic measurement system was developed to measure the temperature dependence more efficiently in millimeter wave range [7].

A measurement apparatus machined from copper in Fig. 1(a) is set in a cryostat and a thermal sensor is attached on the sidewall of a fixed apparatus, as shown in Fig. 11. The AC supply of the cryocooler is turned off to measure  $f_0$  and  $Q_u$  without mechanical vibrations, after it is cooled down from the room temperature to 20 K. Using programs for Windows personal computer developed in our laboratory,  $f_0$  and  $Q_u$  are measured automatically at each 1 K with natural temperature increasing. A program to calculate  $\epsilon_r$  and  $\tan \delta$  from  $f_0$  and  $Q_u$  measured was developed on the basis of Eqs. (1)–(4).

#### 6.2 Measured Results

In advance to measure the temperature dependence of  $\epsilon_r$  and  $\tan \delta$  of plate samples, we need to measure the temperature dependence of  $D$ ,  $H$  and  $\sigma_r$  of the circular empty cavity. The measured results for the TE<sub>011</sub> mode are shown in Fig. 12(a).

The temperature dependence of  $\epsilon_r$  and  $\tan \delta$  of a PTFE plate with  $t=1.073$  mm and coefficient of linear thermal expansion  $\tau_l=100$  ppm/K, a Crythex plate with  $t=0.823$  mm and  $\tau_l=70$  ppm/K and a modified polyolefin, which is named as MPO, plate with  $t=2.050$  mm and  $\tau_l=70$  ppm/K were

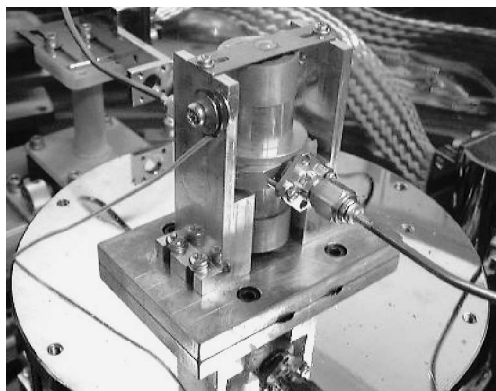


**Fig. 11** Photograph of measurement apparatus attached on a cryostat.

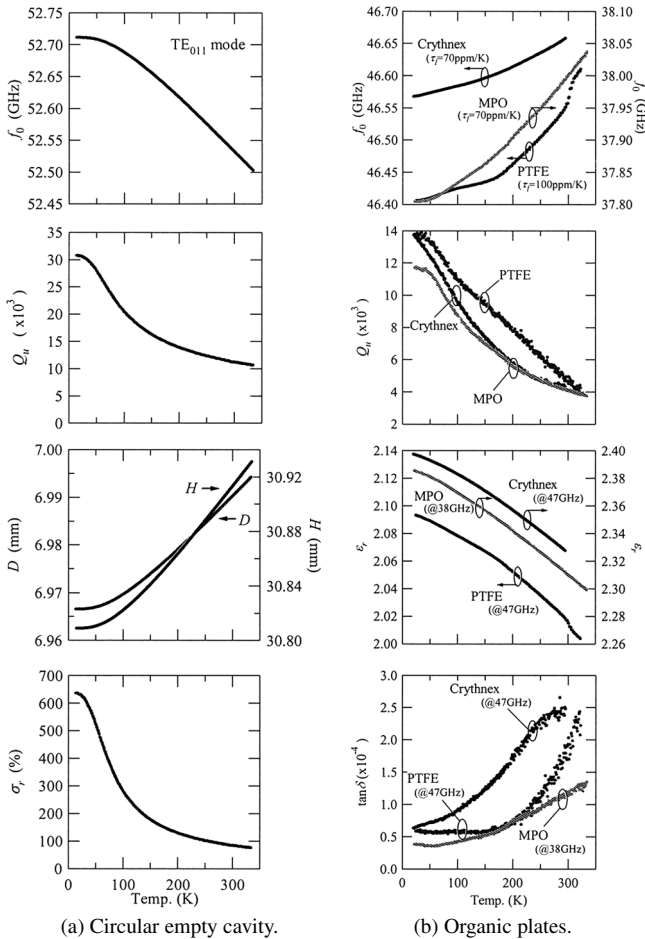


Fig. 12 Temperature dependences of circular empty cavity and PTFE, Crythnex, and MPO plates.

measured for the  $TE_{011}$  mode. The measured results are shown in Fig. 12(b).

The  $f_0$  and  $\epsilon_r$  of the PTFE plate have inflection points near 50 K, 170 K and 290 K, because of the phase transitions of crystal construction. However, the  $f_0$  and  $\epsilon_r$  of the MPO plate have no inflection point. Moreover, the  $\tan \delta$  value of the MPO plate is quite lower than that of the PTFE above room temperature. We can expect that the MPO plates have the high possibility for application to millimeter wave circuit, because of comparable electric characteristics and low price, compared with PTFE plates.

## 7. Conclusion

It was verified that the novel resonator structure proposed in this paper was effective in improvement of accuracy and stability in measurement. As a result, it is concluded that the cut-off circular waveguide method is useful to measure the temperature dependence of complex permittivity of low-loss dielectric plates accurately and efficiently in millimeter wave range. The measurement precisions are estimated within 1 percent for  $\epsilon_r = 2\text{--}30$  and within 15 percent for  $\tan \delta = 10^{-3}\text{--}10^{-6}$ .

## Acknowledgements

The authors wish to thank Mr. M. Kato for his assistance in the measurement. This work is supported in part by the Grant-in-Aid for Scientific Research (KAKENHI14550318) from the Ministry of Education, Culture, Sports, Science and Technology of Japan.

## References

- [1] A.L. Cullen and P.K. Yu, "The accurate measurement of permittivity by mean of an open resonator," Proc. Roy. Soc. A, vol.325, pp.493–509, 1971.
- [2] Y. Kogami, H. Tamura, and K. Matsumura, "Measurements of complex permittivities in 100 GHz band by the Whispering-gallery mode resonator method," IEICE Trans. Electron. (Japanese Edition), vol.J84-C, no.8, pp.703–706, Aug. 2001.
- [3] Y. Ishikawa, T. Tanizaki, A. Saitoh, and T. Yoneyama, "Complex permittivity measurement of dielectric materials using NRD guide at millimeter wave length," IEICE Trans. Electron. (Japanese Edition), vol.J78-C-I, no.9, pp.418–429, Sept. 1995.
- [4] Y. Kobayashi and J. Sato, "Nondestructive measurement of complex permittivity of dielectric plate materials by a cavity resonance method," IEICE Technical Report, MW87-53, Oct. 1987.
- [5] Y. Kobayashi and J. Sato, "Complex permittivity measurement of dielectric plates by a cavity resonance method," IEICE Technical Report, MW88-40, Nov. 1988.
- [6] Y. Kobayashi and T. Shimizu, "Millimeter wave measurements of temperature dependence of complex permittivity of dielectric plates by a cavity resonance method," 1999 IEEE MTT-S Int. Microwave Symp. Digest, pp.1885–1888, June 1999.
- [7] T. Shimizu and Y. Kobayashi, "Millimeter wave measurements of temperature dependence of complex permittivity of GaAs plates by a circular waveguide method," 2001 IEEE MTT-S Int. Microwave Symp. Digest, THIF-51, pp.2195–2198, June 2001.
- [8] T. Shimizu and Y. Kobayashi, "Millimeter wave measurements of some low-loss dielectric plates by a novel cut-off circular waveguide method," 32nd European Microwave Conf. Proc., pp.825–828, Sept. 2002.
- [9] T. Shimizu, Z. Ma, and Y. Kobayashi, "Design of a grooved circular cavity for dielectric substrate measurements in millimeter wave region," IEICE Trans. Electron., vol.E86-C, no.8, pp.1715–1720, Aug. 2003.
- [10] G. Zhang, S. Nakaoka, and Y. Kobayashi, "Millimeter wave measurements of temperature dependence of complex permittivity of dielectric plates by the cavity resonance method," 1997 Asia Pacific Microwave Conf. Proc., pp.913–916, Dec. 1997.
- [11] S.B. Cohn and K.C. Kelly, "Microwave measurement of high-dielectric constant materials," IEEE Trans. Microw. Theory Tech., vol.MTT-14, no.6, pp.406–410, Sept. 1966.
- [12] Y. Kobayashi and T. Hataguchi, "Millimeter wave measurement of complex permittivity by dielectric disk resonator method," 9th International Conf. Infrared and Millimeter Waves Digest, TH4-8, pp.374–375, Oct. 1985.
- [13] G. Kent, "An evanescent-mode tester for ceramic dielectric substrates," IEEE Trans. Microw. Theory Tech., vol.36, no.10, pp.1451–1454, Oct. 1988.
- [14] T. Shimizu, T. Nishino, and Y. Kobayashi, "Some discussions of the resonator structure for the cut-off waveguide method and the round robin test," 33rd European Microwave Conf. Proc., P2-39, pp.755–758, Oct. 2003.
- [15] D. Kajfetz, "Incremental frequency rule for computing the Q-factor of a shielded  $TE_{0mp}$  dielectric resonator," IEEE Trans. Microw. Theory Tech., vol.MTT-32, no.8, pp.941–943, Aug. 1984.

- [16] Y. Kobayashi, T. Aoki, and Y. Kabe, "Influence of conductor shields on the Q-factors of a TE<sub>0</sub> dielectric resonator," IEEE Trans. Microw. Theory Tech., vol.MTT-33, no.12, pp.1361-1366, Dec. 1985.

## Appendix

### A.1 Analysis of Resonance Frequency $f_0$

Figure A·1 shows a resonator structure used in this rigorous analysis. The circular cylinder is cut into two parts in the middle of the height  $H$ . A dielectric plate having relative permittivity  $\varepsilon_r$ , thickness  $t$  and diameter  $d$ , which is a larger size than the diameter of the cylinder  $D$ , is sandwiched between two dielectric supports having relative permittivity  $\varepsilon_g$  and thickness  $g$ . They are placed the two cup-shaped circular cylinders. This structure corresponds to Fig. A·1 when  $g=0$ . The relative permeability  $\mu_r=1$  is assumed in each medium. When  $g \neq 0$  in this configuration, we can calculate the conductor loss at the cavity fringe by the perturbation of  $g$  [15], [16].

The TE<sub>0m1</sub> resonance mode can be analyzed rigorously by the Ritz-Galerkin method. From the structural symmetry, it is sufficient to consider only the region  $0 \leq z \leq H_1$ . The region is divided into three homogeneous subregions [I], [II], and [III]. The quantities for the subregions are denoted by subscripts 1, 2, and 3, respectively. A time harmonic factor  $e^{j\omega t}$  is omitted. Applying the boundary conditions on the  $r$ - $\theta$  plane at  $z = 0$  and on the conducting surface. We can expand magnetic Helmholtz vector  $\Pi_m$  for each region as follows:

$$\begin{aligned}\Pi_{m1} &= \sum_{p=1}^{\infty} A_p J_0(k_{r1p}r) \cos \beta_{1p}z \\ \Pi_{m2} &= \sum_{p=1}^{\infty} B_p J_0(k_{r1p}r) \cos \beta_{2p}z \\ &\quad + \sum_{p=1}^{\infty} C_p J_0(k_{r1p}r) \sin \beta_{2p}z \\ \Pi_{m3} &= \sum_{q=1}^{\infty} D_q J_0(k_{r3q}r) \sin \beta_{3q}(H_1 - z)\end{aligned}\quad (\text{A} \cdot 1)$$

where

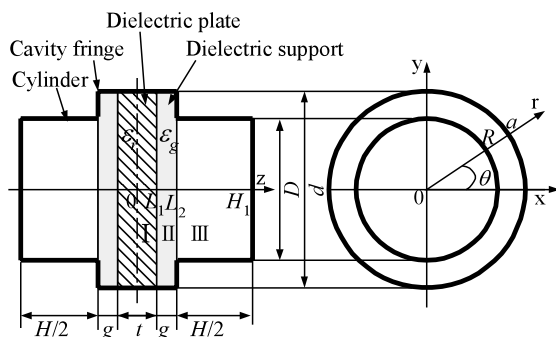


Fig. A·1 Geometry of analysis.

$$\begin{aligned}\beta_{1p}^2 &= \varepsilon_r k_0^2 - k_{r1p}^2 \\ \beta_{2p}^2 &= \varepsilon_g k_0^2 - k_{r1p}^2 \\ \beta_{3q}^2 &= k_0^2 - k_{r3q}^2 \\ k_{r1p} &= u_p/a \\ k_{r3q} &= v_q/R\end{aligned}\quad (\text{A} \cdot 2)$$

In the above,  $A_p$ ,  $B_p$ ,  $C_p$ , and  $D_q$  are expansion coefficients to be determined from the boundary conditions for the regions [I], [II], and [III]. Moreover, the electromagnetic fields components of the TE<sub>0m1</sub> mode in each region are obtained by substituting (A·1) into (A·4).

$$\begin{aligned}H_z &= k^2 \Pi_m + \frac{\partial^2 \Pi_m}{\partial z^2} \\ H_r &= \frac{\partial^2 \Pi_m}{\partial r \partial z} \\ E_\theta &= j\omega\mu_0 \frac{\partial \Pi_m}{\partial r}\end{aligned}\quad (\text{A} \cdot 4)$$

The relationship of  $B_p$  and  $C_p$  is determined from the continuity of  $H_r$  at  $z = L_1$  as follows:

$$\frac{C_p}{B_p} = \frac{\beta_{1p} \tan \beta_{1p} L_1 - \beta_{2p} \tan \beta_{2p} L_1}{\beta_{1p} \tan \beta_{1p} L_1 \tan \beta_{2p} L_1 + \beta_{2p}} \quad (\text{A} \cdot 5)$$

The relationship of  $A_p$  and  $D_q$  is determined from the continuity of  $E_\theta$  and  $H_r$  at  $z = L_2$ . From the former case, we first obtain

$$\begin{aligned}\sum_{p=1}^{\infty} -j\omega\mu_0 A_p k_{r1p} J_1(k_{r1p}r) \\ \cdot (B_p \cos \beta_{2p} L_2 + C_p \sin \beta_{2p} L_2) = E_\theta(r) \\ \sum_{q=1}^{\infty} -j\omega\mu_0 D_q k_{r3q} J_1(k_{r3q}r) \sin \beta_{3q}(H/2) = E_\theta(r)\end{aligned}\quad (\text{A} \cdot 6)$$

where  $E_\theta(r)$  is the  $r$  component of unknown electric field at  $z = L_2$ . Multiplying  $rJ_1(k_{r1p}r)$  on both sides of (A·6) and integrating from 0 to  $a$  with respect  $r$ . Also, multiplying  $rJ_1(k_{r3q}r)$  on both sides of (A·7) and integrating from 0 to  $R$  with respect  $r$ . We obtain the following expressions from the orthogonality of Bessel functions and  $E_\theta(r)=0$  from  $R$  to  $a$ :

$$\begin{aligned}-j\omega\mu_0 A_p k_{r1p} \frac{a^2}{2} \left\{ \begin{array}{l} J_0^2(u_p) \\ J_1^2(u_p) \end{array} \right\} \\ \cdot (B_p \cos \beta_{2p} L_2 + C_p \sin \beta_{2p} L_2) \\ = \int_0^R E_\theta(r) r J_1(k_{r1p}r) dr \\ -j\omega\mu_0 D_q k_{r3q} \sin \beta_{3q}(H/2) \frac{R^2}{2} J_0^2(v_q) \\ = \int_0^a E_\theta(r) r J_1(k_{r3q}r) dr\end{aligned}\quad (\text{A} \cdot 8)$$

From the latter case, we then obtain

$$\begin{aligned}
& \sum_{p=1}^{\infty} A_p k_{r1p} \beta_{2p} J_1(k_{r1p} r) \\
& \quad \cdot (B_p \sin \beta_{2p} L_2 - C_p \cos \beta_{2p} L_2) \\
& = \sum_{q=1}^{\infty} D_q k_{r3q} \beta_{3q} J_1(k_{r3q} r) \cos \beta_{3q} (H/2) \quad (\text{A} \cdot 10)
\end{aligned}$$

Substituting (A·8) and (A·9) into (A·10) to eliminate  $A_p$  and  $D_q$ , multiplying  $rJ_1(k_{r3q}r)$  on both sides and integrating from 0 to  $R$  with respect of  $r$ , we obtain the following integral equation for  $E_{\theta}(r)$ .

$$\begin{aligned}
& \sum_{p=1}^{\infty} \sum_{q=1}^{\infty} \beta_{2p} \frac{\tan \beta_{2p} L_2 - \frac{C_p}{B_p}}{1 + \frac{C_p}{B_p} \tan \beta_{2p} L_2} \frac{P_{pq}}{a^2 \begin{Bmatrix} J_0^2(u_p) \\ J_1^2(u_p) \end{Bmatrix}} \\
& \quad \cdot \int_0^R E_{\theta}(r) r J_1(k_{r1p} r) dr \\
& = \sum_{q=1}^{\infty} \frac{\beta_{3q}}{2} \cot \beta_{3q} (H/2) \int_0^R E_{\theta}(r) r J_1(k_{r3q} r) dr \quad (\text{A} \cdot 11)
\end{aligned}$$

We apply the Ritz-Galerkin method to solve (A·11) by numerical analysis. And expanding  $E_{\theta}(r)$  into an eigenfunction of region [III] as follows,

$$E_{\theta}(r) = \sum_{l=1}^{\infty} E_l J_1(k_{r3l} r), \quad k_{r3l} = \frac{v_l}{R} \quad (\text{A} \cdot 12)$$

where  $E_l$  is an expansion coefficient. Substituting (A·12) into (A·11). Moreover, approximating infinite sum to finite sum, we obtain the following homogeneous equation for  $E_l$  with  $l, q = 1, 2 \dots N, p = 1, 2 \dots K$ .

$$\begin{aligned}
& \sum_{l=1}^N \sum_{q=1}^N \left[ \frac{\delta_{lq} \beta_{3q} R^2 J_0^2(v_q) \cot \beta_{3q} (H/2)}{4} \right. \\
& \quad \left. - \sum_{p=1}^K \frac{\beta_{2p} P_{pq} P_{pl}}{a^2 \begin{Bmatrix} J_0^2(u_p) \\ J_1^2(u_p) \end{Bmatrix}} \frac{\tan \beta_{2p} L_2 - \frac{C_p}{B_p}}{1 + \frac{C_p}{B_p} \tan \beta_{2p} L_2} \right] E_l = 0 \quad (\text{A} \cdot 13)
\end{aligned}$$

For  $E_l$ , which is not zero in (A·13), the determinant of the coefficient matrix needs to be zero. Accordingly, this requirement yields the following  $N \times N$  square determinant with variable  $K$  as a characteristic equation for the  $\text{TE}_{0m1}$  mode.

$$\det H_{lq}(f_0; \varepsilon_r, \varepsilon_g, g, t, d, D, H) = 0 \quad (\text{A} \cdot 14)$$

where the matrix elements  $H_{lq}$  are following

$$H_{lq} = \frac{\delta_{lq}}{4} Y_q J_0^2(v_q) \cot \left( Y_q \frac{(H/2)}{R} \right)$$

$$- \sum_{p=1}^K \frac{Z_p P_{pq} P_{pl}}{a^2 \begin{Bmatrix} J_0^2(u_p) \\ J_1^2(u_p) \end{Bmatrix}} \frac{\tan \left( Z_p \frac{L_2}{R} \right) - \frac{C_p}{B_p}}{1 + \frac{C_p}{B_p} \tan \left( Z_p \frac{L_2}{R} \right)} \quad (\text{A} \cdot 15)$$

$$\begin{aligned}
X_p^2 &= \varepsilon_r (k_0 R)^2 - \left( \frac{R}{a} u_p \right)^2 \\
Z_p^2 &= \varepsilon_g (k_0 R)^2 - \left( \frac{R}{a} u_p \right)^2 \\
Y_q^2 &= (k_0 R)^2 - v_q^2 \quad (\text{A} \cdot 16)
\end{aligned}$$

$$P_{pq} = \frac{v_q J_0(v_q) J_1 \left( \frac{R}{a} u_p \right)}{\left( \frac{R}{a} u_p \right)^2 - v_q^2} \quad (\text{A} \cdot 17)$$

$$P_{pl} = \frac{v_l J_0(v_l) J_1 \left( \frac{R}{a} u_p \right)}{\left( \frac{R}{a} u_p \right)^2 - v_l^2} \quad (\text{A} \cdot 18)$$

Here, in case of subregions [I] and [II] are propagate region and subregions [III] is cut-off region, we obtain following equation,

$$\begin{aligned}
H_{lq} &= \frac{\delta_{lq}}{4} Y_q' J_0^2(v_q) \coth \left( Y_q' \frac{(H/2)}{R} \right) \\
& - \sum_{p=1}^K \frac{Z_p P_{pq} P_{pl}}{a^2 \begin{Bmatrix} J_0^2(u_p) \\ J_1^2(u_p) \end{Bmatrix}} \frac{\tan \left( Z_p \frac{L_2}{R} \right) - \frac{C_p}{B_p}}{1 + \frac{C_p}{B_p} \tan \left( Z_p \frac{L_2}{R} \right)} \quad (\text{A} \cdot 19)
\end{aligned}$$

where

$$Y_q'^2 = v_q^2 - (k_0 R)^2 \quad (\text{A} \cdot 20)$$

Furthermore, we consider height  $H$  is infinite in Eq. (A·19). We obtain following equation,

$$\begin{aligned}
H_{lq} &= \frac{\delta_{lq}}{4} Y_q J_0^2(v_q) \\
& - \sum_{p=1}^K \frac{Z_p P_{pq} P_{pl}}{a^2 \begin{Bmatrix} J_0^2(u_p) \\ J_1^2(u_p) \end{Bmatrix}} \frac{\tan \left( Z_p \frac{L_2}{R} \right) - \frac{C_p}{B_p}}{1 + \frac{C_p}{B_p} \tan \left( Z_p \frac{L_2}{R} \right)} \quad (\text{A} \cdot 21)
\end{aligned}$$

As a result, the resonance frequency for the  $\text{TE}_{0m1}$  mode is calculated by Eq. (1).

## A.2 Analysis of Quality Factor $Q$

Furthermore, the unloaded  $Q$ ,  $Q_u$  is given by

$$\frac{1}{Q_u} = \frac{1}{Q_c} + \frac{1}{Q_d} \quad (\text{A} \cdot 22)$$

where  $Q_c$  and  $Q_d$  are the quality factors due to the conductor loss and the dielectric loss, respectively. The  $Q_c$  is given by

$$\frac{1}{Q_c} = \frac{1}{Q_{cy}} + \frac{1}{Q_{cg}} \quad (\text{A} \cdot 23)$$

where  $Q_{cy}$ , and  $Q_{cg}$  are ones due to the conductor losses of cylinder and cavity fringe, respectively. They are expressed by

$$Q_{cy} = \frac{f_0}{(-\Delta f_{0D}/\Delta D) \delta_c} \quad (\text{A} \cdot 24)$$

$$Q_{cg} = \frac{f_0}{(-\Delta f_{0g}/\Delta g) \delta_c} \quad (\text{A} \cdot 25)$$

$$\delta_c = \frac{1}{\sqrt{\pi f_0 \mu_0 \sigma}} \quad (\text{A} \cdot 26)$$

where  $\delta_c$  is a skin depth,  $\sigma = \sigma_0 \sigma_r$  is the conductivity,  $\sigma_0 = 58 \times 10^6$  S/m is the conductivity of the standard copper, and  $\mu_0 = 4\pi \times 10^{-7}$  H/m is the permeability in the vacuum. Also,  $Q_d$  is given by

$$Q_d = \frac{1}{\tan \delta} \frac{f_0}{2\varepsilon_r \cdot (-\Delta f_{0\varepsilon}/\Delta \varepsilon_r)} \quad (\text{A} \cdot 27)$$

where the resonance frequency change  $\Delta f_{0x}$  due to a small distance change  $\Delta x$  can be calculated from (A·14), where  $x$  is  $D$ ,  $H$ ,  $g$  or  $\varepsilon_r$ . As a result, Eq. (2) is derived from (A·22) to (A·27).



**Takashi Shimizu** was born in Tokyo, Japan, in 1977. He received the B.E. and M.E. degrees in electrical and electronic engineering from Saitama University, Saitama, Japan, in 1999 and 2001, respectively. Now, he is a doctor course student at the same university. His current main interests are measurements of low-loss dielectric materials in microwave and millimeter-wave region. Mr. Shimizu is a student member of the Institute of Electrical and Electronics Engineers.



**Yoshio Kobayashi** was born in Gunma, Japan, in 1939. He received the B.E., M.E., and D.Eng. degrees in electrical engineering from Tokyo Metropolitan University, Tokyo, Japan, in 1963, 1965, and 1982, respectively. Since 1965, he has been with Saitama University, Saitama, Japan. He is now a professor at the same university. His current research interests are in dielectric resonators and filters, measurements of low-loss dielectric and high-temperature superconductive (HTS) materials, and HTS filters,

in microwave and millimeter wave region. He served as the Chair of the Technical Group on Microwaves, IEICE, from 1993 to 1994, as the Chair of the Technical Group of Microwave Simulators, IEICE, from 1995 to 1997, as the Chair of Technical Committee on Millimeter-wave Communications and Sensing, IEE Japan, from 1993 to 1995, as the Chair of Steering Committee, 1998 Asia Pacific Microwave Conference (APMC'98) held in Yokohama, as the Chair of the National Committee of APMC, IEICE from 1999 to 2000, and as the Chair of the IEEE MTT-S Tokyo Chapter from 1995 to 1996. He also serves as a member of the National Committee of IEC TC49 since 1991, the Chair of the National Committee of IEC TC49 WG10 since 1999 and a member of the National Committee of IEC TC90 WG8 since 1997. Prof. Kobayashi received the Inoue Harushige Award on "Dielectric filters for mobile communication base stations" in 1995. He is a Fellow of IEEE and a member of IEE Japan.